# Non-Invasive Optoelectronic System for Color-Change Detection in Oranges to Predict Ripening by Using Artificial Neural Networks

J. D. Filoteo-Razo ⓘ, J. C. Elizondo-Leal ⓘ, J. R. Martinez-Angulo ⓘ, J. H. Barron-Zambrano ⓘ,
A. Díaz-Manriquez ⓘ, V. P. Saldivar-Alonso ⓘ, *Member, IEEE*, J. M. Estudillo-Ayala ⓘ, and R. Rojas-Laguna ⓘ

*Abstract*—The use of sensors to detect or measure ripening changes in fruit is a growing area of interest to the scientific community. Colorimeters are commonly employed for color and shade identification; however, their usage to measure the color parameters of fruit rinds based on image analysis can be expensive. This article presents a non-invasive and low-cost optoelectronic system for detecting color changes in oranges to predict the ripening stage. The system utilises a 1 W white LED as a light source, an RGB photodiode array, and two plastic optical fibres bundled in parallel to form the head of an extrinsic sensor. A microcontroller is employed for model integration and data acquisition. The evolution of the skin color of the fruit was monitored until over-ripeness was evident. The sensor was designed to detect the color changes; the CIE $L*a*b*$ color difference between the optoelectronic device results and those obtained by colorimetry was 2.6–4.5. To predict the ideal conditions for fruit handling and determine the maturity level, a multilevel perceptron ANN was trained, achieving an accuracy of 96.4%. In addition, an overall precision of 96.6% was achieved when classifying fruit into three maturity categories (under-ripe, ripe, and over-ripe), and the error was 3.4%. The combination of the optoelectronic device and ANN improves considerably this fruit color classification accuracy, can facilitate the determination of the optimal time for consumption, and optimize the postharvest process efficiency.

*Index Terms*—Agritech, artificial neural network, citrus orange, fruit ripeness, fibre optic sensors, light reflection, optimum harvest date.

## I. INTRODUCTION

ESTABLISHING the optimum harvest date (OHD) for perishable food is crucial in the agricultural industry. For many commercially produced fruits and vegetables, one parameter that indicates the freshness and flavour of produce is surface color, which can be monitored during harvest and transportation as the fruit ripens. This parameter has been used to evaluate the maturity of many fruits, including tomatoes, bananas, apples, pears, and oranges. In the citrus fruit family, oranges are non-climacteric fruit; that is, they do not continue to ripen after harvest. This characteristic makes their picking date immensely significant [1], [2], [3], [4], [5], [6]. Although color alteration serves as a ripeness indicator, citrus fruits might need to be harvested when ripe yet still green. This is attributed to elevated nocturnal temperatures and an overabundance of nitrogen. In such conditions, the impacted citrus fruits are subjected to a degreening process within ripening chambers, utilising a 2% ethylene environment [7], [8]. This procedure is predominantly employed for international markets such as Canada and Europe. Overall, color change in citrus fruits (e.g., orange, pomelo, lemon, grapefruit, and easy peeler) is a reliable indicator of maturation and OHD [9]; however, there remains a possibility of ripe but still green fruit.

Usually, inspection of surface color to determine the ripening stage of fruit is performed manually: changes in the color and physical structure of fruits (caused by heat, atmospheric water, and biochemical changes) are subjectively analysed to deduce the quality and ripeness of the fruit. The continuous physical changes and accompanying color changes that occur in the fruit-ripening process are usually unpredictable [10], [11]. Compared to manual methods, automated measurements can be more objective, albeit invasive. Non-invasive objective techniques such as spectrometry [12], [13] have been employed to monitor color changes, supplementing invasive techniques that measure variations in the liquid, ethanol, starch, and sugar contents of fruits [14]. In contrast, non-invasive or non-destructive analytical techniques for measuring fruit ripening include various types of imaging, including red, green, and blue (RGB), thermal, hyperspectral, and fluorescence imaging [12], [13], [14], [15], [16], [17]. Each of these imaging techniques utilises a camera that collects light intensity information at a particular wavelength or over a certain wavelength range, which is then processed by a computer.

Various state-of-the-art non-invasive techniques exist for detecting ripening in fruits, often based on the measurement of spectral bands to identify the optimal conditions for fruit harvesting [21], [22]. In [23], the use of a pulse-amplitude

J. D. Filoteo-Razo, J. C. Elizondo-Leal, J. R. Martinez-Angulo, J. H. Barron-Zambrano, A. Díaz-Manriquez, and V. P. Saldivar-Alonso are with the Facultad de Ingeniería y Ciencias, Universidad Autónoma de Tamaulipas, Matamoros, Tamaulipas 87000, México (e-mail: darazo@uat.edu.mx; jcaelizondo@docentes.uat.edu.mx; jrangulo@docentes.uat.edu.mx; hbarron@docentes.uat.edu.mx; amanriquez@docentes.uat.edu.mx; vpsaldiv@docentes.uat.edu.mx).

J. M. Estudillo-Ayala and R. Rojas-Laguna are with the Departamento de Electrónica, División de Ingenierías CIS, Comunidad de Palo Blanco, Universidad de Guanajuato, Salamanca, Guanajuato 36885, Mexico (e-mail: julian@ugto.mx; rlaguna@ugto.mx).

Digital Object Identifier 10.1109/JPHOT.2023.3312212

modulated fluorometer to evaluate changes in the chlorophyll content of the golden papaya fruit was reported, and the results were compared with those obtained using a digital penetrometer to assess firmness and a colorimeter to assess skin color. The study revealed an important correlation between the techniques, which could be used to help verify overall fruit quality through complementary and non-invasive methods. In [24], it was reported that the combination of reflectance and fluorescence spectroscopy could be utilised to quantify changes in chlorophyll and other chromophores during the ripening of papayas, nectarines, mangoes, and guavas. In the same study, gas in scattering media absorption spectroscopy, based on tuneable diode-laser absorption spectroscopy at 760 nm, was employed to measure the content of free molecular oxygen in fruit tissue.

On the other hand, mid-infrared (MIR) spectroscopy, a non-invasive method that can be used to measure firmness, peel thickness, and total pectin [25], has been demonstrated to be capable of determining fruit quality. This approach facilitates production planning, which ensures that the produce meets market standards. However, this method, which requires constant monitoring and verification at each stage of ripening, is time- and labour-intensive. Furthermore, improper handling practices, such as pounding, pressing, throwing, and rubbing the product during long harvesting days, can cause irreversible damage to the fruit. An alternative non-invasive method is the use of the partial least-squares regression models of time-domain nuclear magnetic resonance (NMR) relaxometry and spectroscopic data from near-infrared (NIR) spectroscopy [26]. NIR and MIR spectroscopies have also been utilised for the analysis of vitamin C, citric acid, total sugars, and reducing agents in this type of fruit [27]. Additionally, a new ultrasonic method using frequencies lower than 200 kHz has been employed to evaluate the quality (amount of water, density) of citric fruits such as oranges [25], where the reflections at the interface of the fruit and the ultrasonic transducer were analysed, and a high correlation was obtained between the firmness of the orange and the measurements acquired by the ultrasonic device.

The study in [29] explored an innovative sensor technology for the non-destructive determination and prediction of the OHD in cherries. Fruit quality was assessed using weight and fruit size parameters. However, these parameters were found to be insufficient indicators of OHD due to their variability with crop load, climatic conditions, cultural practices, and seasons. To address this limitation, the study utilised a sensor to monitor fruit pigmentation change, observing coloration changes through a spectrometer before and after harvest. The instrument featured five light-emitting diodes (LEDs) arranged in a ring as light-emitting sources, with a central detector measuring the light spectrum in the 400–1100 nm range emitted by the fruit peel. This device was used to track chlorophyll degradation, detect ripening, and predict the OHD for cherries. Because this device uses an optical spectrum analyser, it can be expensive and sensitive to interference and noise, potentially affecting the accuracy and reliability of the data obtained.

Advances in computer technology and deep learning-based detection techniques have also been used to detect the ripening stage. Artificial neural networks (ANNs) can process
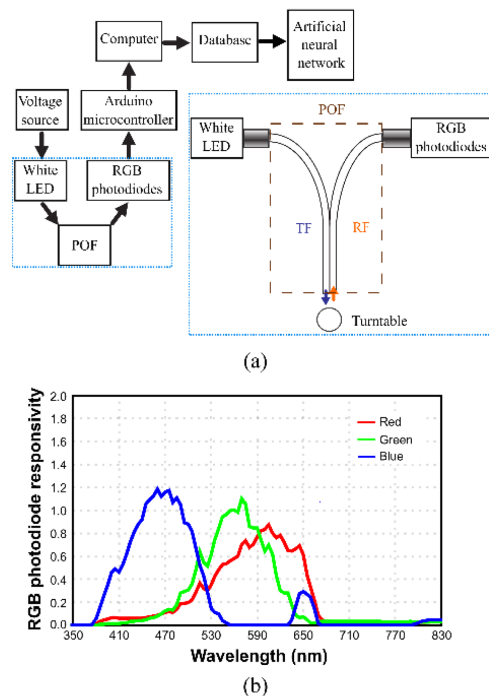


Fig. 1. (a) Block diagram of the color-sensing device. POF: Plastic optical fibre. TF: Transmitting fibre. RF: Receiving fibre. (b) Normalised R, G, and B spectral response of ISL29125 transducer [35].

image data for fruit classification. These networks, which emulate the function of biological neural networks, have been applied to the problems of data classification, pattern recognition, and behaviour prediction. A type of ANN called a multilayer perceptron backpropagation algorithm has been used for fruit color classification [26], [27], [28], color-shade identification, surface-bruise, and damage identification [29], as well as the classification of different types of fruit according to extracted image features [30]. Another ANN variant, the back-propagation neural network (BPNN) model, has been applied in the field of pesticide residue detection to ensure safe consumption of produce such as fruits and vegetables [31]. Moreover, the study in [36] used an image analysis with a BPNN for early-yield prediction, presenting an effective approach to forecast fruit yields using machine vision and machine learning for apples, with potential applicability to other fruit crops.

Owing to the high cost of thermal, hyperspectral, and fluorescence cameras and the time required for image processing and color analysis of the fruit, we focus on RGB photodiode detection, which is a low-cost technique [37], [38], [39]. This method extracts information from reflected light using three coupled photodiodes that separate it into its RGB components [32]. Although color changes can be evaluated using commercial equipment, such instruments are typically expensive and difficult for farmers to access. The objective of this study was to evaluate the potential of a color-detection technique using a non-invasive and low-cost optoelectronic device with a white-light emitting diode system as a light source, a plastic optical fibre (POF) as an extrinsic sensor, and RGB photodiodes as light decoders for

interpretation in a digital system. Here, a prototype instrument for the estimation of fruit quality (color changes in harvested oranges) is presented and compared to commercial equipment in terms of cost and usability. Additionally, the classification and prediction capabilities of ANNs for RGB color analysis of fruit samples are discussed. This device is demonstrated to be a viable substitute for contemporary methods used in fruit ripening, such as image processing vision techniques, spectral analysis, or odour analysis devices. This system incorporates cost-effective electronic and POF components that enable swift identification of the ripening stage of oranges by means of a non-invasive technique. Also, the combination of an optoelectronic system and ANNs offers advantages such as higher prediction accuracy, processing automation and efficiency, adaptability to different fruit varieties and conditions, and the ability to learn and continuously improve from the system. These advantages render this combination a promising tool for the task of fruit sorting and prediction, especially in the context of postharvest efficiency and timely fruit consumption.

## II. MATERIALS AND METHODS

### A. Experimental Setup

The experimental setup of a non-invasive and low-cost opto-electronic system scheme proposed for color-change detection in oranges is shown in Fig. 1(a). The device consists of a white light source, a 1 W white LED (Siled, model LED-P1W100-120/41) powered by a +5 V source, a POF (Industrial Fiber Optics, model FB140-1-ND) waveguide for the extrinsic sensor, and transducer with RGB photodiodes (Renesas, model ISL29125 [35]) containing three photodiode arrays that convert light into electric current with spectral-sensitivity peaks at approximately 620 (red), 565 (green), and 485 (blue) nm, respectively. The ISL29125 detector is designed to reject infrared wavelengths from light sources, enabling the device to operate in environments ranging from sunny outdoors to dark rooms [35]. Fig. 1(b) shows the normalised spectral response of the RGB photodiodes in the ISL29125 sensor, according to the sensor datasheet [35]. The POF is composed of polymethylmethacrylate resin with a refractive index of 1.49 (numerical aperture = 0.5); the core and outer diameters are 980 and 1000 µm, respectively. It consists of a transmitting fibre, which carries the radiation emitted by the light source to the surface of the orange being tested [36], and a receiving fibre, which carries the light subsequently reflected by the sample to the RGB photodiodes. After the light transmitted to the diodes is converted into electric current during the light-to-signal process, the current output is converted into a digital count by an on-chip analogue-to-digital converter, which has a conversion resolution selectable between 12 or 16 bits.

The RGB color values were collected in a database to enable the subsequent extraction of information about each color channel. The mean, variance, and standard deviation were calculated. Thus, an RGB color-model matrix was generated in the database. Because the manual rotation of the fruit by the user could cause misalignment when performing color measurements at each position, the data-capture process was automated using a turntable to rotate the fruit to each specific angle; Fig. 2(a)
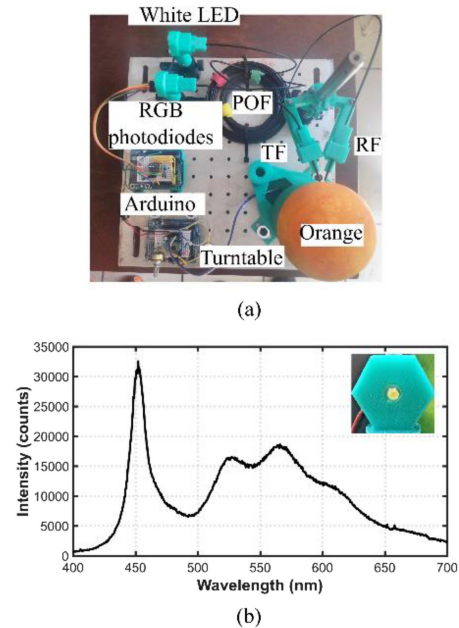


(a)



(b)

Fig. 2. (a) Experimental setup viewed from above. POF: Plastic optical fibre. TF: Transmitting fibre. RF: Receiving fibre. (b) Transmission spectrum of the LED used as a white light source.

TABLE I
MEASURED RGB-SCALE VALUES FOR A HALF-WHITE, HALF-BLACK SPHERE

| Colour | R | G | B |
|--------|-----|------|-----|
| White | 764 | 1069 | 506 |
| Black | 67 | 69 | 55 |

provides an overview of the experimental setup. All the devices were mounted on an optical table (30 × 30 cm, 2.54 cm grid), which allowed the distances between the optical components to be adjusted. Measurements were acquired during continuous rotation of the turntable in discrete steps. The transmission spectrum was measured using an optical spectrum analyser (Ocean Optics, model USB2000+), as shown in Fig. 2(b).

### B. Testing and Calibration of the Color-Sensing Device

A spherical, half-white, half-black object was used to calibrate the equipment and placed on the turntable. From a fixed starting point, it rotated continuously while 200 measurements in one complete revolution were taken at regular intervals to cover 360° (resolution: 1.8°). Table I lists the resulting RGB values. The measurement of the light reflected by the colorless (black) surface corresponds to the least intense signal that the RBG photodiode sensor can detect, and that of the white surface corresponds to the most intense. Fig. 3 shows the calibration graph. The RGB values, as shown in Fig. 3, were normalised into the range 0 to 255, with white (255, 255, 255) and black (0, 0, 0) on the RGB scale; note that the values shown in Table I are the raw un-normalised values. By averaging the measurements, a grey color (127.5, 127.5, and 127.5 in RGB values) is obtained, as shown in the inset in Fig. 3.
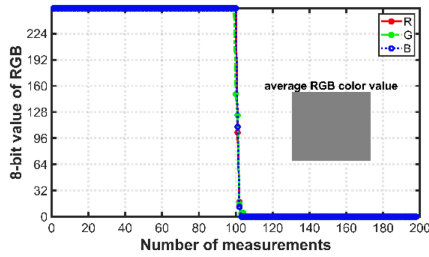
Fig. 3.   Calibration with a half-white, half-black sphere. White has an RGB value of (255, 255, 255); black has an RGB value of (0, 0, 0).

### C. Comparison of Color Measurements Obtained With Colorimeter and Optoelectronic Device

To test the color measurement of the device, a database of color information for 210 oranges obtained with a colorimeter (Konica Minolta, model C400) and photographs taken with a digital camera (Canon, model EOS 550D) from COFILAB (www.cofilab.com) was used. This database contained photographs and colorimetry results at different stages of ripening for each of the 210 oranges, which were analysed to determine the degreening status of each of the fruits in terms of its citrus color index (CCI) [37]. Degreening is a postharvest treatment that accelerates the disappearance of the green color from citrus peel and the manifestation of the underlying coloration provided by carotenoid pigments, whose synthesis, in turn, can be accelerated. The purpose of this technique is to be able to market a fruit that has reached the degree of coloration demanded by the consumer but has not met the requirement of maturity appropriate for consumption. The CCI can be calculated using the following equation:

$$CCI = \frac{1000 \times a*}{L* \times b*}, \tag{1}$$

where $L*$, $a*$, and $b*$ are the variables of the International Commission on Illumination (CIE) $L*a*b*$ system ($L*$ denotes lightness, $a*$ denotes the red–green value, and $b*$ denotes the yellow–blue value) [37]. Table II compares the colorimetry measurements obtained from the COFILAB database and those obtained from the optoelectronic device, using the COFILAB photographs as samples, for seven stages of ripening. A significant difference between the values obtained via RGB color analysis and CCI is apparent: for the first sample, using the optoelectronic device, an average CCI of −19.67 ($L* = 40.20$, $a* = −13.82$, and $b* = 17.47$) was obtained based on 100 measurements, whereas a CCI in the range from −14.39 to −15.90 (average CCI = −14.42) was obtained from the colorimetry data (see Table II). Consequently, the result for our device is within a reliable range of the colorimetry results. Similarly, we can determine the total color difference between the CIE $L*a*b*$ system coordinates for the two results using the following equation:

$$\Delta E* = \sqrt{\Delta L*^2 + \Delta a*^2 + \Delta b*^2}, \tag{2}$$

where $\Delta L*$, $\Delta a*$, and $\Delta b*$ are the color difference variables of the CIE $L*a*b*$ system [37]. $\Delta E*$ is within the range of 2.6–4.5 for each of the samples shown in Table II. This range

of $\Delta E*$ can be used to assess the color tolerance, to determine whether the difference between the color values obtained using the optoelectronic device and colorimetry is sufficiently small. Thus, the orange color-evaluation process can be validated: the range of $\Delta E*$ obtained is not large; therefore, the results for the developed device can be considered acceptable.
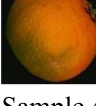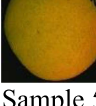
### D. Data Collection

Fruit color datasets must be collected under controlled conditions; for example, an ambient temperature of 25 °C should be maintained and a light source with known parameters should be used. Therefore, the data collection was performed in a room with an encapsulation unit for the light source white and RGB photodiodes fabricated using a 3D printer (Makerbot, model Replicator+). This printer can create three-dimensional solid objects using molten polylactic acid filament. The data obtained from the RGB photodiodes were the input data for the ANN in this study. Data were obtained on the change in coloration, hue, saturation, and illumination of oranges using a three-color RGB model (the values obtained from the RGB photodiodes). Additionally, hue, saturation, and value (HSV) and CIE $L*a*b*$ models, called color spaces, were used to obtain information about the aforementioned changes. For example, image analysis methods utilise the segmentation of images acquired during fruit ripening; however, this visual method is not effective due to its sensitivity to illumination condition changes and light obstruction [39]. To avoid these problems, different color spaces have been used to extract the information from the object under study using combinations of color spaces, such as RGB, HSV, and CIE $L*a*b*$ [40], [41]. Here, the color space that best mimics the way colors are perceived in human vision was sought. Humans identify the color of an object through its chromaticity and luminosity [2]. The CIE $L*a*b*$ space was designed to be a perceptually uniform space, and its perception is close to that of the human eye. However, the HSV space coordinates indicate the intensity, lightness, and brightness of the color [42]. Therefore, these three-color spaces (RGB, HSV, and CIE $L*a*b*$) were all used in this study. Five oranges that had recently arrived at the supermarket were acquired and analysed over a period of 30 days. For each orange, approximately 82000 measurements per day were obtained while it rotated on the turntable, illuminated by a cold white LED. Because the starting point is fixed and the rotation is continuous, 200 measurements were acquired during each rotation of the turntable (one complete revolution). Therefore, 410 measurements of the average color per revolution were obtained per day (82000/200 = 410 per revolution). For each of the three color models, for the three oranges, three statistical values (the mean, variance, and standard deviation) were determined; hence, a 410 × 3 matrix of result data was obtained.

## III. ANN ARCHITECTURE

### A. ANN

The primary objective of an ANN is to identify patterns within a given dataset. Comprised of individual neurons, an ANN

TABLE II
COMPARISON BETWEEN MEASUREMENTS IN CIE L∗A∗B∗ SPACE OBTAINED USING KONICA MINOLTA C400 COLORIMETER AND OPTOELECTRONIC DEVICE

| Sample | Colourimeter C400 | | | | Optoelectronic device | | | | $\Delta E^*$ |
|---|---|---|---|---|---|---|---|---|---|
| | $L^*$ | $a^*$ | $b^*$ | CCI | $L^*$ | $a^*$ | $b^*$ | CCI | |
| Sample 1 | 38.4 | −9.6 | 17.4 | −14.4 | 40.2 | −13.8 | 17.4 | −19.6 | 4.5 |
| Sample 2 | 44.7 | −12.3 | 22.1 | −12.5 | 43.2 | −14.9 | 23.1 | −15.0 | 3.2 |
| Sample 3 | 49.4 | −3.6 | 26.7 | −2.8 | 51.3 | −4.0 | 29.6 | −2.6 | 3.4 |
| Sample 4 | 59.7 | 23.6 | 36.0 | 10.9 | 60.1 | 25.5 | 37.8 | 11.2 | 2.6 |
| Sample 5 | 59.4 | 8.5 | 35.5 | 3.9 | 62.2 | 10.3 | 37.8 | 4.3 | 4.0 |
| Sample 6 | 66.5 | 17.0 | 40.5 | 6.2 | 68.1 | 19.9 | 42.3 | 6.9 | 3.7 |
| Sample 7 | 65.1 | 16.5 | 39.6 | 6.3 | 68.2 | 18.7 | 41.4 | 6.6 | 4.1 |
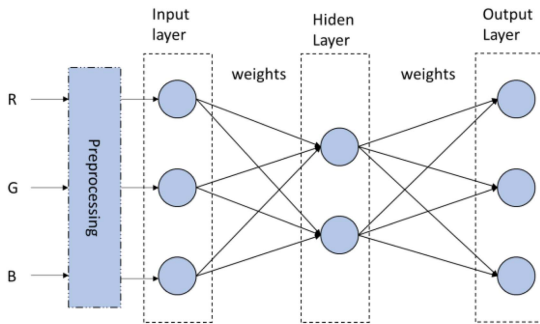


Fig. 4. Architecture of multilayer ANN.

comprises an input layer, a weight vector, an activation function, and an output layer. In our project, we utilised a multilayer perceptron (MLP), which underwent training with three layers (Fig. 4): an input layer consisting of three neurons, a hidden layer with two neurons, and an output layer comprising three neurons.

Each input neuron represents a specific RGB color level, whereas the neurons in the output layer correspond to the ripeness level of the fruit.

Each neuron in the hidden layer and in the output layer obtains its value from the weights $w$, the value of the neurons in the previous layer, and the activation function $\Phi$, which is defined using the following equation:

$$\Phi = \Phi_a \left( \sum_{j=1}^{m} w_{ij}\sigma_i + b_i \right), \qquad (3)$$

where $m$ is the number of neurons in the previous layer, $w_{ij}$ is the associated weight of neuron $i$ to neuron $j$, $\sigma_i$ is the $i$th neuron, $b_i$ is the bias of the $i$th neuron, and $\Phi_a$ is the activation function.

B. Training Algorithms

Scikit-learn was used for preprocessing, network training, and data classification [43]. To configure an ANN, preprocessing,

Fig. 5. High repeatability of the test measurement using an orange color sample.

initialisation of the weights, and configuration of the hyperparameters must all be performed. Because the MLP is sensitive to data size, it is rec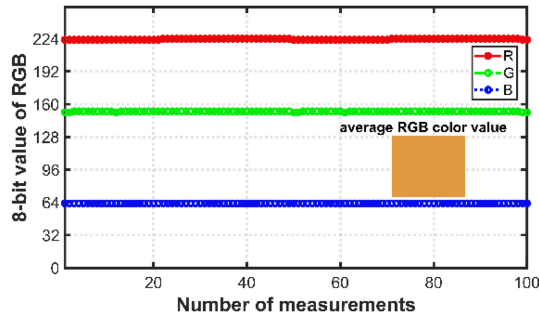ommended to scale the input data of the network [44]; therefore, we chose to standardise the input R, G, and B data. In other words, the input data were scaled such that their mean was 0 and standard deviation was 1. The standard score of a sample $x$ is given by the following equation:

$$I = \frac{x - u}{s}, \qquad (4)$$

where $u$ and $s$ are the mean and standard deviation of the training samples, respectively.

## IV. RESULTS AND DISCUSSION

First, we investigated the repeatability of the measurements of the optoelectronic system. For this purpose, we measured the color of a color sample. For each sample, 100 measurements were performed, as shown in Fig. 5. These results demonstrate that this type of RGB transducer has an accuracy similar to the accuracies of other conventional methods [45], [46]. These measurements may exhibit an error that is uniformly distributed due to the discretisation noise in the internal analogue-to-digital conversion of the RGB transducer. Additionally, to improve the repeatability of the measurements, calibration must be performed by the end user, and such calibration results may differ depending on the specific RGB sensor used; indeed, small color differences have been found between the measurements performed using other RGB color sensors and spectrometers.

Fig. 6 shows histograms of the measured RGB color values for oranges over the entire 30 days of the monitoring period. The normal distribution function of the RGB colors during ripening changes is shown by the grey bars, whereas the overlaid colored lines are fitted normal distributions for specific days in the data collection period. The data in the histograms for the three color coordinates start shifting to the right, towards lighter colors (green–yellow), and then to the left, towards darker colors (0, 0, 0) as the measurement period increases. Therefore, the maturation is uniform across the samples during the 30-day monitoring period. This result shows that color change information can also be obtained using RGB color space to study the degree of ripeness in fruits using the RGB transducer, together with the POF, and it demonstrates that this color measurement
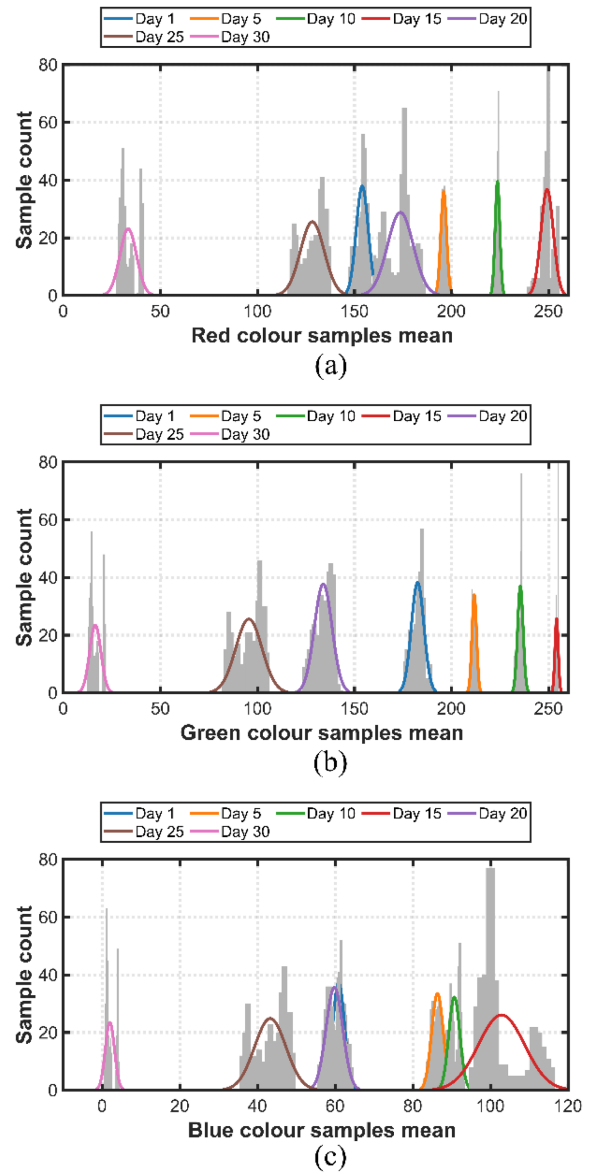


Fig. 6. Histograms (grey bars) with overlaid fitted normal distributions (colored lines) of the measured RGB color values of oranges over the 30-day monitoring period: (a) R, (b) G, and (c) B histograms.

information obtained is better. In addition, a previous study showed that other color scales such as the HSV scale allow better appreciation of the color variation, based on hue, saturation, and value, for accurate determination of the degree of ripeness [1]. In the present study, conversion from RGB into HSV color was used to observe the color variation; however, the results we obtained demonstrate that this is not necessary, because the color variation over the test period is apparent in the graph.

In our study, during the 30-day measurement period, 12046 data elements were collected, of which 9636 were used for training and 2410 for validation. From the data processed for training the neural network, the mean of each input datum (RGB) was obtained as $\bar{u} = [182.3 \ 181.3 \ 71.2]$ and the standard deviation as $\bar{s} = [69.3 \ 83.2 \ 33.8]$. The training solver is the limited-memory

TABLE III
WEIGHTS W FROM THE INPUT LAYER TO THE HIDDEN LAYER

|  | $h_1$ | $h_2$ |
|---|---|---|
| $I_1$ | 6.7 | −6.6 |
| $I_2$ | −28.2 | −23.3 |
| $I_3$ | −3.9 | 9.0 |

TABLE IV
WEIGHTS W FROM THE HIDING LAYER TO THE OUTPUT LAYER

|  | $v_1$ | $v_2$ | $v_3$ |
|---|---|---|---|
| $h_1$ | −17.0 | −2.7 | 19.4 |
| $h_2$ | 22.5 | −13.1 | −8.8 |

Broyden–Fletcher–Goldfarb–Shanno (L-BFGS) algorithm [47]. Among the parameters to be configured in the neural network is the activation function of the neurons of the hidden layer, for which the rectified linear unit (*ReLu*) function was chosen [53]. The *ReLu* function is defined as $\Phi_h(y) = \max(0, y)$, where *y* is the input of the activation function. As there are three output neurons, the *softmax* activation function [49] was chosen in the output layer. In effect, the *softmax* function performs a normalisation of the input data vector $\bar{v} = [v_1, \ldots, v_k]$ to a probability distribution, and the neuron that will be activated will be the one corresponding to the highest probability. The equation to obtain the *softmax* function for the *i*th output is

$$\Phi_v(\bar{v})_i = \frac{e^{v_i}}{\sum_{j=1}^{k} e^{v_j}} \forall_i \in \{1, \ldots, k\}. \tag{5}$$

After MLP training, a network with the weights from input layer *I* to hidden layer *h* was obtained as shown in Table III.

The weights of each neuron in the hidden layer *h* to each neuron in the output layer *v* are shown in Table IV.

The biases for the hidden layer nodes $h_1$ and $h_2$ are $bh_1 = 12.0$ and $bh_2 = 15.5$, respectively, whereas the biases for the output layer nodes $v_1$, $v_2$, and $v_3$ are $bv_1 = -9.4$, $bv_1 = 5.4$, and $bv_3 = 3.1$, respectively. The Accuracy (Ac), Precision (P), rCall, F1-score, and confusion matrix [54] were used to evaluate the performance of the proposed method. Given the true positive, true negative, false positive, and false negative counts (TP, TN, FP, and FN, respectively), we can obtain each of our metrics from the equations:

$$Ac = \frac{TP + TN}{TP + TN + FP + FN}, \tag{6}$$

$$P = \frac{TP}{TP + FP}, \tag{7}$$

$$rCall = \frac{TP}{TP + FN}, \tag{8}$$

$$F1 = 2\frac{P \times rCall}{P + rCall}. \tag{9}$$

TABLE V
RCALL, F1-SCORE, AND PRECISION METRICS OBTAINED USING THE PROPOSED SYSTEM

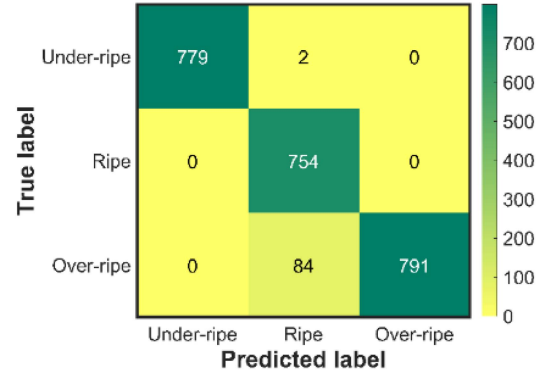| Class | Precision | rCall | F1-Score |
|---|---|---|---|
| Under-ripe | 1.0 | 0.9 | 0.9 |
| Ripe | 0.8 | 1.0 | 0.9 |
| Over-ripe | 1.0 | 0.9 | 0.9 |
| Macro avg | 0.9 | 0.9 | 0.9 |
| Weighted avg | 0.9 | 0.9 | 0.9 |



Fig. 7. Confusion matrix for the test data produced by the proposed system.

From the experiments conducted, Ac = 0.9 was obtained, and Table V shows the Ac, rCall, and F1-Score metrics, which demonstrate very good performance for the classification of fruit maturity using the proposed optical sensor. This finding shows that the values obtained by the classifier are optimal results for the classification of the color change of an orange by the optoelectronic system during the process of optimal consumption time determination.

Fig. 7 shows the confusion matrix of the test data produced by the proposed system. Here, TP and TN are much higher than FP, and for the under-ripe class, TP is 779 and FN is only 2; however, in the ripe class, TP is 754. The incorrectly classified cases indicate the potential ripening days of each orange in relation to the change in its evaluated characteristics because each fruit undergoes a different ripening process. This finding leads to the hypothesis that the color characteristics of the oranges are continuously and significantly changing with the passing of days in terms of their classification; in this study, the ANN analysis facilitated more accurate and efficient classification. In addition, the incorrect classification cases are related to the change in the size of the orange during the test period, owing to weight loss caused by dehydration as the color of the fruit changes.

A comparison of the optoelectronic–ANN technique developed by us with other previously used techniques for color measurement and ripening classification in oranges is presented in Table VI; our system has an accuracy of 96.4%. Therefore, this device can function as a suitable alternative to modern image processing vision techniques, spectral analysis, or odour analysis devices in the assessment of fruit ripening. In addition, it consists of low-cost electronic and POF elements, and it can discern the

TABLE VI
COMPARISON OF OUR SYSTEM WITH PREVIOUSLY REPORTED SYSTEMS FOR ASSESSING THE RIPENING OF ORANGES USING ANNs

| Fruit | Classification algorithm | Analysis techniques | Detector | Accuracy (%) | Precision (%) | Ref. |
|---|---|---|---|---|---|---|
| Orange | Decision tree | Image processing | Digital camera | 93.1 | 93.4 | [55] |
| Orange | Multilayer perceptron | Spectrometer data | Headspace gas chromatography–mass spectrometry | 82 ± 1 | - | [56] |
| Orange | Hybrid artificial neural network – harmony search | Image processing | Digital camera | 96.7 | - | [57] |
| Orange | Support vector machine and decision tree | Image processing | Digital camera | 87.8 | - | [58] |
| Orange | Keras neural network library | data fruit odour data | Electronic nose | ≥ 95 | 95 | [59] |
| Orange | Logistic regression | Image processing | Digital camera | 97 | - | [60] |
| **Orange** | **Multilayer Perceptron** | **RGB colour data** | **Optoelectronic system** | **96.4** | **96.6** | **This work** |

ripening stage of oranges rapidly. These findings demonstrate that the ANN we used has a good classification range for determining the level of ripeness of an orange and can also determine the number of days left before it is ready for optimal consumption. To improve the proposed method, more RGB color data would need to be obtained from oranges at different stages of ripeness to increase the classification capability of the RGB photodiode technique. In addition, a larger number of training patterns would be required, resulting in more time-consuming training and classification. Notably, acquiring the values in the database using the RGB photodiodes was faster than obtaining images using a camera, owing to the time required for image processing in the latter case. While color change is a reliable indicator of maturity in citrus fruits, the degreening practice shows that maturity is also influenced by various internal factors and growing conditions. Rapid degreening can occasionally lead to a decrease in fruit quality. Such fruits may not develop the same level of flavour, sweetness, and aroma as those that ripen naturally on the tree. Textural changes, such as softening or increased susceptibility to bruising, may also occur. The opto-electronic system presented in this article should facilitate the technological development and implementation of measurement and control systems linked to ANNs for the inspection of fruit ripening and quality. The POF offers high flexibility, vibration resistance, and durability. Furthermore, it has advantages such as insensitivity to electromagnetic waves, no heat generation, and easy, low-cost fabrication. This system could replace the manual fruit sorting process in small-scale industrial fruit production. The use of optoelectronic devices and ANN learning offers improvements in the efficacy of sorting fruit to assess the optimal time for consumption, ensuring timely consumption, and enables postharvest efficiency to be assessed. This system has the potential to be employed for a variety of fruits, considering that numerous immature green fruits are subjected to a chlorophyll breakdown process to attain the desired color that consumers find appealing.

## V. CONCLUSION

In this study, a non-invasive and low-cost optoelectronic system was developed to detect color changes in oranges and predict the ripening stage; comparing the results obtained using this system with those obtained using a conventional colorimetry system, the total color difference was 2.6–4.5. By using the POF together with the other plastic components of the fabricated system, it was ensured that the signal detected by the RGB transducer was stable, even when an external light source caused interference. A multilayer perceptron was employed to predict suitable conditions for fruit handling and the ripening stage of the fruit with an accuracy of 96.4%, a precision of 96.6%, and an error of 3.4%. The solver for training was L-BFGS. The advantage of our proposed ANN-based system is that the data acquired for training are distinct from those used for image processing. Taking advantage of this characteristic, we developed a system for directly capturing sample data using RGB color coordinates. Use of the optoelectronic system should facilitate the implementation of measurement and control systems that incorporate ANNs to inspect the quality of fruit ripening. The as-developed method achieved a 96.6% success rate based on a comparison of stored data with the results of classifying the color status of the fruit. Our ANN method, together with the optoelectronic system, offers improved classification times in comparison with photographic methods, which are slower because they require image processing. To increase the success rate of the ANN, a greater number of fruit RGB measurements must be acquired to compile a larger database. Further research will focus on other

neural network architectures and algorithms. Moreover, in the future, to improve the performance of the training algorithms and extend their applicability to other fruits (or similar areas), classification based on fruit features, such as principal color, fruit diseases, and quality, is a possibility. This device could be used for several other fruits, considering many immature green fruits are subjected to chlorophyll degradation to attain the color that appeals to consumers.

## REFERENCES

[1] A. Lazaro, M. Boada, R. Villarino, and D. Girbau, "Color measurement and analysis of fruit with a battery-less NFC sensor," *Sensors*, vol. 19, no. 7, 2019, Art. no. 1741.

[2] W. M. Syahrir, A. Suryanti, and C. Connsynn, "Color grading in tomato maturity estimator using image processing technique," in *Proc. IEEE 2nd Int. Conf. Comput. Sci. Inf. Technol.*, 2009, pp. 276–280.

[3] P. Das, J. K. P. S. Yadav, and L. Singh, "Deep learning-based tomato's ripe and unripe classification system," *Int. J. Softw. Innov.*, vol. 10, no. 1, pp. 1–20, 2022.

[4] C. Kim et al., "A phage-and colorimetric sensor-based artificial nose model for banana ripening analysis," *Sensors Actuators B Chem.*, vol. 362, 2022, Art. no. 131763.

[5] A. Bhargava and A. Bansal, "Grading of variety of bi and mono-colored ApplesT," in *Soft Computing and Signal Processing*. Berlin, Germany: Springer, 2022, pp. 375–382.

[6] B. Demir, N. Çetin, and Z. A. Kuş, "Determination of color properties of weed using image processing," *Alinteri J. Agriculture Sci.*, vol. 31, no. 2, pp. 59–64, 2016.

[7] M. Agustí, C. Mesejo, C. Reig, and A. Martínez-Fuentes, "Citrus production," in *Horticulture: Plants for People and Places, Volume 1: Production Horticulture*, Berlin, Germany: Springer, 2014, pp. 159–195.

[8] V. Serna-Escolano, M. J. Giménez, M. E. García-Pastor, A. Dobón-Suárez, S. Pardo-Pina, and P. J. Zapata, "Effects of degreening treatment on quality and shelf-life of organic lemons," *Agronomy*, vol. 12, no. 2, 2022, Art. no. 270.

[9] L. Zacarias, P. J. R. Cronje, and L. Palou, "Postharvest technology of citrus fruits," in *The Genus Citrus*. Amsterdam, The Netherlands: Elsevier, 2020, pp. 421–446.

[10] M. A. Buitrago, "Manejo de manzanas en cosecha y poscosecha," *Bioplasma*, vol. Documentos, Núm. IV, p. 12, 1991.

[11] E. Raj, M. Appadurai, and K. Athiappan, "Precision farming in modern agriculture," in *Smart Agriculture Automation Using Advanced Technologies*, Berlin, Germany: Springer, 2021, pp. 61–87.

[12] A. Carrillo-López and E. M. Yahia, "Changes in color-related compounds in tomato fruit exocarp and mesocarp during ripening using HPLC-APcI+-mass Spectrometry," *J. Food Sci. Technol.*, vol. 51, no. 10, pp. 2720–2726, 2014.

[13] T. Ringer and M. Blanke, "Non-invasive, real time in-situ techniques to determine the ripening stage of banana," *J. Food Meas. Characterization*, vol. 15, pp. 4426–4437, 2021.

[14] L. S. Magwaza and U. L. Opara, "Analytical methods for determination of sugars and sweetness of horticultural products—A review," *Sci. Horticulturae*, vol. 184, pp. 179–192, 2015.

[15] G. Bai, S. Jenkins, W. Yuan, G. L. Graef, and Y. Ge, "Field-based scoring of soybean iron deficiency chlorosis using RGB imaging and statistical learning," *Front. Plant Sci.*, vol. 9, 2018, Art. no. 1002.

[16] W. Yuan, N. K. Wijewardane, S. Jenkins, G. Bai, Y. Ge, and G. L. Graef, "Early prediction of soybean traits through color and texture features of canopy RGB imagery," *Sci. Rep.*, vol. 9, no. 1, pp. 1–17, 2019.

[17] G. Bodner, A. Nakhforoosh, T. Arnold, and D. Leitner, "Hyperspectral imaging: A novel approach for plant root phenotyping," *Plant Methods*, vol. 14, no. 1, pp. 1–17, 2018.

[18] I. Chandrasekaran, S. S. Panigrahi, L. Ravikanth, and C. B. Singh, "Potential of near-infrared (NIR) spectroscopy and hyperspectral imaging for quality and safety assessment of fruits: An overview," *Food Anal. Methods*, vol. 12, no. 11, pp. 2438–2458, 2019.

[19] A. Siedliska, P. Baranowski, M. Zubik, W. Mazurek, and B. Sosnowska, "Detection of fungal infections in strawberry fruit by VNIR/SWIR hyperspectral imaging," *Postharvest Biol. Technol.*, vol. 139, pp. 115–126, 2018.

[20] N. Ekramirad et al., "Nondestructive detection of codling moth infestation in apples using pixel-based NIR hyperspectral imaging with machine learning and feature selection," *Foods*, vol. 11, no. 1, 2022, Art. no. 8.

[21] A. Lai, E. Santangelo, G. P. Soressi, and R. Fantoni, "Analysis of the main secondary metabolites produced in tomato (Lycopersicon esculentum, Mill.) epicarp tissue during fruit ripening using fluorescence techniques," *Postharvest Biol. Technol.*, vol. 43, no. 3, pp. 335–342, 2007.

[22] Y. Wu, L. Li, L. Liu, and Y. Liu, "Nondestructive measurement of internal quality attributes of apple fruit by using NIR spectroscopy," *Multimedia Tools Appl.*, vol. 78, no. 4, pp. 4179–4195, 2019.

[23] I. U. Bron, R. V. Ribeiro, M. Azzolini, A. P. Jacomino, and E. C. Machado, "Chlorophyll fluorescence as a tool to evaluate the ripening of 'Golden' papaya fruit," *Postharvest Biol. Technol.*, vol. 33, no. 2, pp. 163–173, 2004.

[24] H. Zhang, J. Huang, T. Li, X. Wu, S. Svanberg, and K. Svanberg, "Studies of tropical fruit ripening using three different spectroscopic techniques," *Proc. SPIE*, vol. 19, no. 6, 2014, Art. no. 67001.

[25] M. Bizzani, D. W. M. Flores, L. A. Colnago, and M. D. Ferreira, "Non-invasive spectroscopic methods to estimate orange firmness, peel thickness, and total pectin content," *Microchemical J.*, vol. 133, pp. 168–174, 2017.

[26] Y. Liu, X. Sun, and A. Ouyang, "Nondestructive measurement of soluble solid content of navel orange fruit by visible–NIR spectrometric technique with PLSR and PCA-BPNN," *LWT-Food Sci. Technol.*, vol. 43, no. 4, pp. 602–607, 2010.

[27] K. R. Borba, P. C. Spricigo, D. P. Aykas, M. C. Mitsuyuki, L. A. Colnago, and M. D. Ferreira, "Non-invasive quantification of vitamin C, citric acid, and sugar in 'Valência'oranges using infrared spectroscopies," *J. Food Sci. Technol.*, vol. 58, no. 2, pp. 731–738, 2021.

[28] D. S. Morrison and U. R. Abeyratne, "Ultrasonic technique for non-destructive quality evaluation of oranges," *J. Food Eng.*, vol. 141, pp. 107–112, 2014.

[29] V. Overbeck, M. Schmitz, and M. Blanke, "Non-destructive sensor-based prediction of maturity and optimum harvest date of sweet cherry fruit," *Sensors*, vol. 17, no. 2, 2017, Art. no. 277.

[30] N. Kumari, A. K. Bhatt, R. K. Dwivedi, and R. Belwal, "Hybridized approach of image segmentation in classification of fruit mango using BPNN and discriminant analyzer," *Multimedia Tools Appl.*, vol. 80, no. 4, pp. 4943–4973, 2021.

[31] S. Ghazal, W. S. Qureshi, U. S. Khan, J. Iqbal, N. Rashid, and M. I. Tiwana, "Analysis of visual features and classifiers for fruit classification problem," *Comput. Electron. Agriculture*, vol. 187, 2021, Art. no. 106267.

[32] S. Abirami and M. Thilagavathi, "Classification of fruit diseases using feed forward back propagation neural network," in *Proc. Int. Conf. Commun. Signal Process.*, 2019, pp. 0765–0768.

[33] P. Maniwara, K. Nakano, D. Boonyakiat, S. Ohashi, M. Hiroi, and T. Tohyama, "The use of visible and near infrared spectroscopy for evaluating passion fruit postharvest quality," *J. Food Eng.*, vol. 143, pp. 33–43, 2014.

[34] Y. Zhang, S. Wang, G. Ji, and P. Phillips, "Fruit classification using computer vision and feedforward neural network," *J. Food Eng.*, vol. 143, pp. 167–177, 2014.

[35] H. Bian et al., "Multiple kinds of pesticides detection based on back-propagation neural network analysis of fluorescence spectra," *IEEE Photon. J.*, vol. 12, no. 2, Apr. 2020, Art. no. 6801009.

[36] H. Cheng, L. Damerow, Y. Sun, and M. Blanke, "Early yield prediction using image analysis of apple fruit and tree canopy features with neural networks," *J. Imag.*, vol. 3, no. 1, 2017, Art. no. 6.

[37] J. D. Filoteo-Razo et al., "RGB color sensor implemented with LEDs," *Proc. SPIE*, vol. 9571, pp. 144–149, 2015, doi: 10.1117/12.2188243.

[38] J. D. Filoteo-Razo et al., "Sensor RGB para detectar cambios de color en piel de frutas," *Acta Universitaria*, vol. 26, no. 1, pp. 24–29, 2016.

[39] R. Damayanti, Y. Hendrawan, B. Susilo, and S. Oktavia, "Prediction of tomatoes maturity using TCS3200 color sensor," in *Proc. Inst. Phys. Conf. Ser.: Earth Environ. Sci.*, 2020, Art. no. 012011.

[40] ISL29125, "Digital red, green and blue color light sensor with IR blocking filter," *Renesas*, pp. 1–17, 2017. Accessed: Apr. 22, 2022. [Online]. Available: https://www.renesas.com/www/doc/datasheet/isl29125.pdf

[41] P. Kishore, D. Dinakar, and M. Padmavathi, "Fiber optic vibration sensors," in *Optoelectronics*, London, U.K.: IntechOpen, 2021.

[42] M. Jiménez-Cuesta, J. Cuquerella, and J. M. Martinez-Javaga, "Determination of a color index for citrus fruit degreening," in *Proc. Int. Soc. Citriculture/Int. Citrus Congr.*, 1981, pp. 1982–1983.

[43] A. M. Saad, A. Ibrahim, and N. El-Bialee, "Internal quality assessment of tomato fruits using image color analysis," *Agricultural Eng. Int.: CIGR J.*, vol. 18, no. 1, pp. 339–352, 2016.

[44] G. Moreira, S. A. Magalhães, T. Pinho, F. N. dos Santos, and M. Cunha, "Benchmark of deep learning and a proposed HSV colour space models for the detection and classification of greenhouse tomato," *Agronomy*, vol. 12, no. 2, 2022, Art. no. 356.

[45] Q. Feng, X. Wang, G. Wang, and Z. Li, "Design and test of tomatoes harvesting robot," in *Proc. IEEE Int. Conf. Inf. Automat.*, 2015, pp. 949–952.

[46] A. Arefi, A. M. Motlagh, K. Mollazade, and R. F. Teimourlou, "Recognition and localization of ripen tomato based on machine vision," *Australian J. Crop Sci.*, vol. 5, no. 10, pp. 1144–1149, 2011.

[47] I. Kurniastuti, E. N. I. Yuliati, F. Yudianto, and T. D. Wulan, "Determination of hue saturation value (HSV) color feature in kidney histology image," *J. Phys.: Conf. Ser.*, vol. 2157, 2022, Art. no. 12020.

[48] F. Pedregosa et al., "Scikit-learn: Machine learning in Python," *J. Mach. Learn. Res.*, vol. 12, pp. 2825–2830, 2011.

[49] C. C. Aggrawal, *Neural Networks and Deep Learning: A Textbook*. Berlin, Germany: Springer, 2018.

[50] A. Brugiapaglia, G. Destefanis, S. Agosta, and L. Di Stasio, "Repeatability and reproducibility of two instruments to measure meat colour," in *Proc. 62nd Int. Congr. Meat Sci. Thecnol.*, 2016, pp. 1–4.

[51] R. B. Dominguez, M. A. Orozco, G. Chávez, and A. Márquez-Lucero, "The evaluation of a low-cost colorimeter for glucose detection in salivary samples," *Sensors*, vol. 17, no. 11, 2017, Art. no. 2495.

[52] D. C. Liu and J. Nocedal, "On the limited memory BFGS method for large scale optimization," *Math Program.*, vol. 45, no. 1–3, pp. 503–528, 1989.

[53] V. Nair and G. E. Hinton, "Rectified linear units improve restricted Boltzmann machines," in *Proc. 27th Int. Conf. Mach. Learn.*, 2010, pp. 807–814.

[54] N. W. S. Wardhani, M. Y. Rochayani, A. Iriany, A. D. Sulistyono, and P. Lestantyo, "Cross-validation metrics for evaluating classification performance on imbalanced data," in *Proc. Int. Conf. Comput., Control, Inform. Appl.*, 2019, pp. 14–18.

[55] A. Wajid, N. K. Singh, P. Junjun, and M. A. Mughal, "Recognition of ripe, unripe and scaled condition of orange citrus based on decision tree classification," in *Proc. Int. Conf. Comput., Math. Eng. Technol.*, 2018, pp. 1–4.

[56] S. Taghadomi-Saberi, S. Mas Garcia, A. A. Masoumi, M. Sadeghi, and S. Marco, "Classification of bitter orange essential oils according to fruit ripening stage by untargeted chemical profiling and machine learning," *Sensors*, vol. 18, no. 6, 2018, Art. no. 1922.

[57] S. Sabzi, Y. Abbaspour-Gilandeh, and G. García-Mateos, "A new approach for visual identification of orange varieties using neural networks and meta-heuristic algorithms," *Inf. Process. Agriculture*, vol. 5, no. 1, pp. 162–172, 2018.

[58] M. E. Irhebhude, A. O. Kolawole, and F. B. Bugaje, "Recognition of mangoes and oranges colour and texture features and locality preserving projection," *Int. J. Comput. Digit. Syst.*, vol. 11, no. 1, pp. 963–975, 2022.

[59] P. Tyagi, R. Semwal, A. Sharma, U. S. Tiwary, and P. Varadwaj, "E-nose: A low-cost fruit ripeness monitoring system," *J. Agricultural Eng.*, vol. 54, 2022.

[60] M. A. J. Al-Sammarraie et al., "Predicting fruit's sweetness using artificial intelligence—Case study: Orange," *Appl. Sci.*, vol. 12, no. 16, 2022, Art. no. 8233.